Journal of Applied Physics

RESEARCH ARTICLE | JULY 07 2023

Experimental demonstration of superdirective spherical dielectric antenna FREE

Roman Gaponenko ; Mikhail S. Sidorenko ; Dmitry Zhirihin ; Ilia L. Rasskazov ; Alexander Moroz ; Konstantin Ladutenko ; Pavel Belov ; Alexey Shcherbakov

Journal of Applied Physics 134, 014901 (2023)
https://doi.org/10.1063/5.0155677

Journal of Applied Physics ARTICLE pubs.aip.org/aip/jap

Experimental demonstration of superdirective spherical dielectric antenna

Cite as: J. Appl. Phys. **134**, 014901 (2023); doi: 10.1063/5.0155677
Submitted: 22 April 2023 · Accepted: 14 June 2023 ·
Published Online: 7 July 2023

Roman Gaponenko,[1,a)] Mikhail S. Sidorenko,[1] Dmitry Zhirihin,[1] Ilia L. Rasskazov,[2] Alexander Moroz,[3] Konstantin Ladutenko,[1] Pavel Belov,[1] and Alexey Shcherbakov[1]

AFFILIATIONS

[1]School of Physics and Engineering, ITMO University, 197101 St. Petersburg, Russia
[2]KLA Corporation, 5 Technology Drive, Milpitas, California 95035, USA
[3]wave-scattering.com

[a)]**Author to whom correspondence should be addressed:** roman.gaponenko@metalab.ifmo.ru

ABSTRACT

An experimental demonstration of directivities exceeding the fundamental Kildal limit, a phenomenon called *superdirectivity*, is provided for spherical high-index dielectric antennas with an electric dipole excitation. A directivity factor of about 10 with a total efficiency of more than 80% for an antenna having a size of a third of the wavelength was measured. High directivities are shown to be associated with constructive interference of particular electric and magnetic modes of an open spherical resonator. Both analytic solutions for a point dipole and a full-wave rigorous simulation for a realistic dipole antenna were employed for optimization and analysis, yielding an excellent agreement between experimentally measured and numerically predicted directivities. The use of high-index low-loss ceramics can significantly reduce the physical size of such antennas while maintaining their overall high radiation efficiency. Such antennas can be attractive for various high-frequency applications, such as antennas for the Internet of Things, smart city systems, 5G network systems, and others. The demonstrated concept can be scaled in frequency.

I. INTRODUCTION

Utilization of dielectrics as high-Q resonators, which gave birth to the first concepts of all-dielectric antennas,[1–3] has a long history stretching back more than a century ago.[4–7] Such antennas became attractive for various high-frequency applications due to numerous advantages, including small physical size, simplicity of design and production, high temperature tolerance, corrosion resistance, high radiation efficiency, wide frequency range, adaptive polarization, ease of integration with other antennas and multiple feed systems, and stable radiation patterns. This prospect has become appealing with the advent and rapid development of communication networks with a significantly increased amount of transmitted data.[8–11] An increased interest in the application of all-dielectric antennas based on spherical resonators is witnessed in numerous theoretical[12–25,76] and experimental[26–40] works. Antennas made of materials with simultaneously high refractive indices and low losses became increasingly interesting in recent years. Due to a large contrast with the environment, such antennas have small radiation leakage, facilitated by high Q-factors of resonances. In the optical band, high-index dielectric nanoparticles have been employed for enhancing the direction-selective absorption and emission of nanoantennas.[41–43]

The radiation pattern of an antenna is determined by the interference of excited electric and magnetic modes of an open resonator. To obtain a directional design, it is necessary to have constructive mode interference in a given direction and destructive in other directions. The maximum directivity of an antenna is usually considered to be constrained by the so-called Kildal[44,45] limit,

$$\mathcal{D}_{\mathrm{lim}} = (kR_{\mathrm{ant}})^2 + 3. \tag{1}$$

The limit is expressed solely in terms of the antenna "size parameter," kR_{ant}, where R_{ant} is the radius of the sphere circumscribing the antenna and k is the free-space wave number. Note in passing that this limit does not always work for electrically small dielectric antennas.[25,46,47] The antennas that exceed this limit are called

superdirective. It is possible to obtain electrically small superdirective antennas.[48–52] Unfortunately, such antennas become inefficient[53] as their size decreases, because they require relatively high currents to radiate even low powers. Strong currents lead to an increase in Ohmic losses and large reactive fields near the antenna. Even if Ohmic losses can be significantly reduced by using materials with a low-loss tangent (for the resonator, $\tan\delta < 0.001$), the issue of increasing reactive fields is not so easy to resolve. An increase in the dielectric constant of the resonator with decreasing size leads to greater localization of the field of *internal*[23] (or interior[7]) modes inside the resonator and to an increase in sensitivity to the slightest changes inside the resonator antennas (e.g., the location and shape of the feeding element).

In view of the above challenges, it has not been obvious that experimental realization of small superdirective *dielectric* resonant antennas with practical parameters was feasible. In this work, we demonstrate the existence of such designs via numerical optimization and direct measurements. Moreover, we will show that even very simple designs consisting of a homogeneous dielectric sphere fed by an electric dipole source can meet the superdirectivity requirements while retaining a reasonable bandwidth. In what follows, our theoretical approach, experimental details, and measured data are described.

II. METHODS

A. Theory

The main parameters characterizing an antenna are the directivity, $\mathcal{D}$, gain, $\mathcal{G}$, and the realized gain, $\mathcal{G}_\mathcal{R}$. The directivity is a dimensionless parameter determined by a relation of the power emitted in some direction to an average of the emitted power over the full solid angle,

$$\mathcal{D}(\theta,\phi) = \frac{4\pi|F(\theta,\phi)|^2}{\int_0^{2\pi}\int_0^{\pi}|F(\theta',\phi')|^2\sin\theta'\,d\theta'\,d\phi'}. \tag{2}$$

Here, $|F(\theta,\phi)|$ is the normalized radiation pattern. $\mathcal{D}$ is determined solely by the shape of the antenna pattern and does neither take into account the antenna radiation efficiency, e, nor the reflection losses due to an impedance mismatch.

The *gain* of an antenna, $\mathcal{G}$, is related to the directivity by $\mathcal{G} = e_{cd}\mathcal{D}$, where e_{cd} is the antenna radiation efficiency ($0 \le e_{cd} \le 1$). The *realized* gain, $\mathcal{G}_\mathcal{R}$, is the gain of an antenna reduced by its impedance mismatch factor[54] and related to the directivity through the total antenna efficiency ($0 \le e_0 \le 1$) by the formula $\mathcal{G}_\mathcal{R} = e_0\mathcal{D}$. In the measurement setup considered in this work (see Fig. 1), the gain, $\mathcal{G}$, and realized gain, $\mathcal{G}_\mathcal{R}$, can be derived from the Friis transmission equation[55] for the line-of-sight communication between two antennas in a lossless medium (air),[56]

$$\mathcal{G}_\mathcal{R}(\theta,\phi) = \frac{P_{rec}}{P_{tr}}\left(\frac{4\pi r}{\lambda}\right)^2\frac{1}{p\,\mathcal{G}_{rec}(1-|\Gamma_{rec}|^2)}, \tag{3}$$

$$\mathcal{G}(\theta,\phi) = \mathcal{G}_\mathcal{R}(\theta,\phi)/e_r = \mathcal{G}_\mathcal{R}(\theta,\phi)/(1-|\Gamma_{tr}|^2), \tag{4}$$

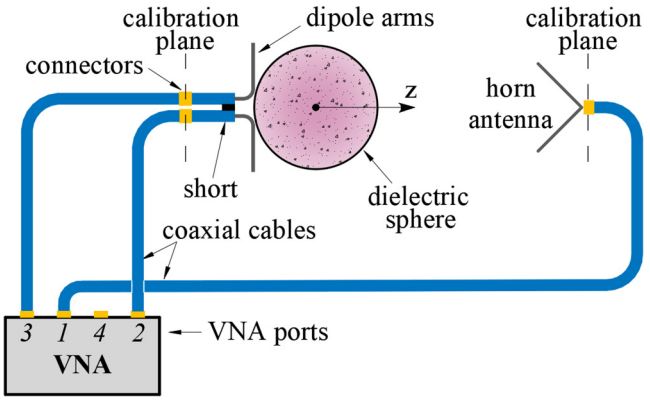

FIG. 1. The scheme of a three-port connection of an experimental setup for the radiation pattern measurement using an R&S ZVB20 vector network analyzer.

where p is the polarization mismatch factor (in our case, $p = 1$), e_r is the reflection (mismatch) efficiency, λ is the free-space wavelength, P_{tr} refers to the power provided to a transmission line attached to an emitting antenna, and P_{rec} refers to the power received from a transmission line attached to a receiving antenna. Γ is the reflection coefficient for an impedance mismatch between the antenna and a transmission line. Subscripts "*tr*" and "*rec*" are used here for the transmitting antenna (the superdirective antenna under study) and the receiving horn antenna. $\mathcal{G}_{rec}$ is the gain of the receiving horn antenna in the direction strictly oriented to the transmitting antenna (measured by the two-antenna method[57]).

A general physical picture of light scattering by a spherical particle under plane wave illumination is well described by the Lorenz–Mie theory,[58] where the solution is represented as an infinite multipole series of partial vector spherical waves. The theory provides an exact solution regardless of the wavelength and the size of the sphere. The Lorenz–Mie theory was later generalized to the case of a point dipole excitation source.[14] Note in passing that such an analytical solution is only available for perfectly spherical surfaces. Any other geometric shapes require more sophisticated numerical methods.[59,60]

The physics underlying resonant scattering behavior of a dielectric resonator is the excitation of its electrical and magnetic modes. Resonant modes of an open spherical resonator can be found from exact analytical formulas for a homogeneous sphere.[7,58] For the respective $\mathrm{TE}_{\ell mq}$ and $\mathrm{TM}_{\ell mq}$ modes, these formulas are

$$\begin{aligned}\frac{j_{\ell-1}(\eta_1 kR_1)}{j_\ell(\eta_1 kR_1)} &= \frac{h^{(2)}_{\ell-1}(kR_1)}{\eta_1 h^{(2)}_\ell(kR_1)},\\ \frac{\ell}{\eta_1 kR_1} - \frac{j_{\ell-1}(\eta_1 kR_1)}{j_\ell(\eta_1 kR_1)} &= \frac{\eta_1\ell}{kR_1} - \eta_1\frac{h^{(2)}_{\ell-1}(kR_1)}{h^{(2)}_\ell(kR_1)}.\end{aligned} \tag{5}$$

Here, j_ℓ and $h^{(2)}_\ell$ are the usual spherical Bessel function of the first kind and the spherical Hankel function of the second kind,[61] respectively, ℓ stands for multipole order, index q labels the subsequent roots of Eq. (5), $\eta_1 = \sqrt{\varepsilon_1}$ is the refractive index of the

sphere material, R_1 is the radius of the homogeneous sphere, and k is a free-space wavenumber. The equations above are independent of the azimuthal mode number m due to the spherical symmetry. All $2\ell + 1$ modes with different m are degenerate in frequency.[7]

For spherical resonators with a high refractive index, approximate conditions for excitation of the electric $TM_{\ell mq}$ and magnetic $TE_{(\ell+1)mq}$ modes are closely related. They can be roughly estimated in the limit $\eta_1 \to \infty$, in which case Eq. (5) reduces to

$$j_\ell(\zeta_{\ell q}) \simeq 0, \tag{6}$$

with $\zeta_{\ell q} = \eta_1 k R_1$ being the qth zero of the ℓth order spherical Bessel functions of the first kind j_ℓ (see Table I). An approximate equation (6) can be used for a quick and easy estimate of the frequency position of the relevant resonator modes.

At the first stage of this work, initial designs with high directivity were obtained by performing optimization using the analytical solution for a sphere excited by a point electric dipole.[14] In order to precisely match the experiment, subsequent optimization was performed in the CST Studio Suite[62] taking into account a *finite* and realistic dipole size and connector cables. During optimization, our search for optimal parameters of the dipole was performed by varying (i) the position of the dipole, (ii) the thickness and length of the dipole arms, (iii) their offset and bend radius, and (iv) the distance between the dipole arms. A frequency shift of resonance was achieved, if required, by changing either the resonator permittivity or its size. The above approach allowed us to obtain the designs of directional antennas with high total antenna efficiency under realistic conditions, closely matching the experiment.

B. Experimental setup and measurements

Experimental measurements of the directivity were carried out in an anechoic chamber using an R&S®ZVB20 vector network analyzer (VNA). The horn antenna was mounted on a triaxial positioner. The antenna under study was located on a special foam pedestal on a rotary positioner (see photographs in Sec. I of the supplementary material). As indicated in Fig. 1, experimental data were obtained using a three-port connection to the VNA by measuring the S-parameters in the planes $\phi = 0°$ and $\phi = 90°$ with a θ angle step of 1° (see Sec. II of the supplementary material). The secant plane of $\phi = 0°$ includes the z axis and the arms of the dipole, while the plane of $\phi = 90°$ is perpendicular to the arms of the dipole.

TABLE I. Zeros $\zeta_{\ell q}$ of the spherical Bessel function of the first kind $j_\ell(\zeta_{\ell q} = \eta_1\ k\ R_1) = 0$. The subscript q denotes here the ordinal number of the zero of the ℓth order spherical Bessel function.

	$q = 1$	$q = 2$	$q = 3$	$q = 4$
$\ell = 0$	3.141 59	6.283 19	9.424 78	12.5664
$\ell = 1$	4.493 41	7.725 25	10.904 1	14.0662
$\ell = 2$	5.763 46	9.095 01	12.322 9	15.5146
$\ell = 3$	6.987 93	10.417 1	13.698	16.9236
$\ell = 4$	8.182 56	11.704 9	15.039 7	18.3013
$\ell = 5$	9.355 81	12.966 5	16.354 7	19.6532

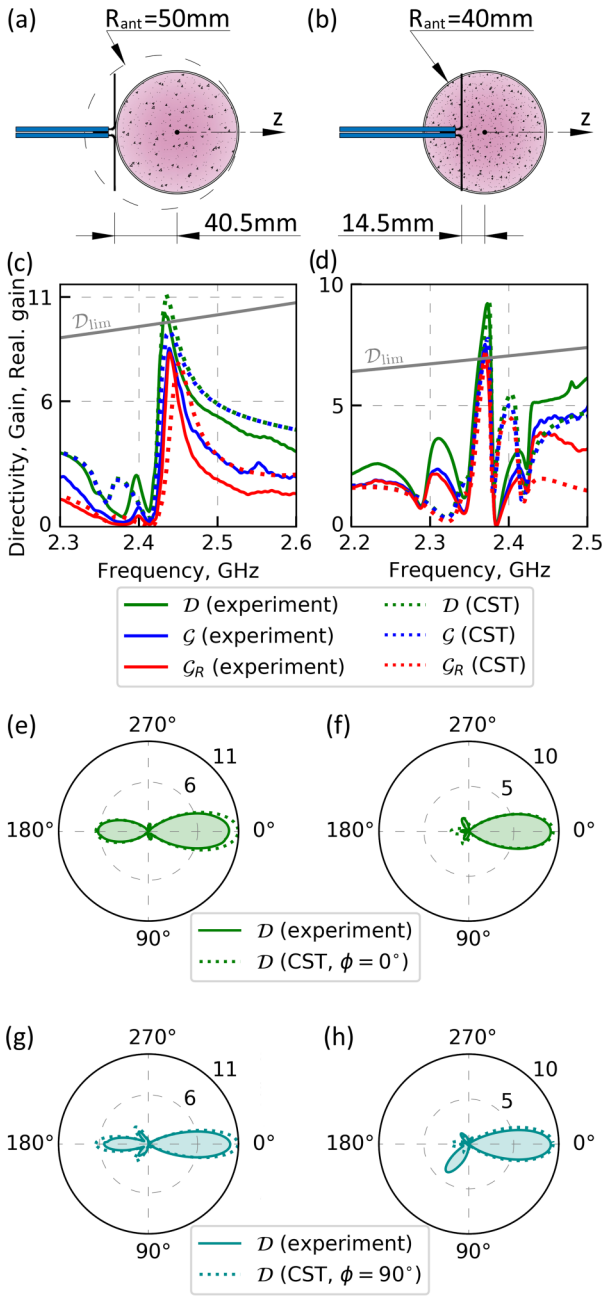

FIG. 2. (a) and (b) Schematic representation of our antennas in the form of a dielectric sphere excited by an (a) externally and (b) internally placed electric dipole. The radii of circumscribing spheres are 50 mm and 40 mm, respectively. (c) and (d) Dependence of directivity $\mathcal{D}$, gain $\mathcal{G}$, and realized gain $\mathcal{G}_\mathcal{R}$ in the forward direction as a function of frequency for the respective antennas shown in (a) and (b). (e)–(h) Dependence of the directivity on the angle θ in the planes $\phi = 0°$ and $\phi = 90°$ at the frequencies 2.433 and 2.373 GHz (in a linear scale) corresponding to the maximum values of directivity of the antenna in the respective column. Numbers on concentric circles in the polar plots reflect corresponding directivity values.

The measurements were carried out within a 1.4–2.6 GHz band with a frequency resolution of 1 Hz. The antenna under study was located in the far field of the horn antenna at a distance of 3 m. To implement an electric dipole, two coaxial cables $RG-58\ A/U$ with a characteristic impedance of $50 \pm 2\,\Omega$ located side by side were used. The arms of the dipole were made from the inner conductors of coaxial cables with a diameter of 1 mm. As illustrated in Fig. 1, the horn antenna was connected to the physical port 1 of the VNA, which was represented by a logical port $s1$. The physical ports 2 and 3 were connected to the dipole arms and combined into a differential logical port $d2$.

The quantity S_{s1d2} describing the transmission from the balanced port with differential mode stimulus $d2$ to the single-ended port $s1$ was measured in the experiment. The radiation pattern $|F(\theta, \phi)|$ in Eq. (2) is determined as $|S_{s1d2}(\theta, \phi)|$ divided by $\max(|S_{s1d2}(\theta, \phi)|)$, where the maximum is taken over all possible angular directions. The ratio P_{rec}/P_{tr} in Eq. (3) is equal to the measured value $|S_{s1d2}|^2$. The reflection coefficients for each antenna are $\Gamma_{rec} = S_{s1s1}$ and $\Gamma_{tr} = S_{d2d2}$. In general, all the S-parameters can be obtained by measuring reflection and transmission between individual ports in accordance with the theory describing multiport experimental measurements,[63,64]

$$S = \begin{bmatrix} S_{s1s1} & S_{s1d2} & S_{s1c2} \\ S_{d2s1} & S_{d2d2} & S_{d2c2} \\ S_{c2s1} & S_{c2d2} & S_{c2c2} \end{bmatrix} = \frac{1}{2} \begin{bmatrix} 2S_{11} & \sqrt{2}(S_{12} - S_{13}) & \sqrt{2}(S_{12} + S_{13}) \\ \sqrt{2}(S_{21} - S_{31}) & S_{22} - S_{23} - S_{32} + S_{33} & S_{22} + S_{23} - S_{32} - S_{33} \\ \sqrt{2}(S_{21} + S_{31}) & S_{22} - S_{23} + S_{32} - S_{33} & S_{22} + S_{23} + S_{32} + S_{33} \end{bmatrix}, \tag{7}$$

where the subscript "s" stands for the single mode, "d" for the differential mode, and "c" for the common mode.

III. RESULTS

A. External dipole

In order to achieve the superdirective regime, we first considered a dipole located near a spherical resonator—a system that might be one of the most interesting ones from a practical viewpoint and the simplest one for an experimental implementation. The dielectric antenna was made in the form of a plastic ball filled with ceramic powder and excited externally by an electric dipole as shown in Fig. 2(a). The length of the dipole arms is 38 mm, and the gap between the centers of the cables supplying the dipole is ~4 mm. The plastic shell made of acrylic with a thickness of ~1.1 mm has an outer radius $R_2 = 40$ mm, the real part of permittivity $\varepsilon_2' \simeq 1.7$, and the loss tangent $\tan\delta_2 \simeq 0.02$. Free flowing dielectric powder ECCOSTOCK HiK has the real part of permittivity $\varepsilon_1' \simeq 12.2$ and the loss tangent $\tan\delta_1 \simeq 0.0007$. Vibrations were used to obtain dense packaging of the ceramic powder inside the spherical resonator.

The plastic shell is used in this work to maintain the shape of the resonator, and has been taken into account in all our calculations. The thickness of the dielectric shell is ~40 times less than the radius of the sphere filled with dielectric powder. Given that the characteristics of the shell are much closer to air than to the powder, the results with and without the plastic shell appear pretty much the same (see Sec. IV of the supplementary material).

At the first stage, an interval containing the frequencies of the first eigenmodes of a homogeneous spherical resonator was considered. Figure 3 shows a comparison of the directivity calculated analytically for a sphere excited by a tangentially oriented point dipole with the results obtained by the full-size simulation in CST Studio Suite and measured experimentally. Experimental results agree well with the simulations. At the same time, the analytical point dipole model[14] describes quite well the position and magnitude of jumps in the directivity. Such Fano-type[36] directivity behavior near resonant frequencies arises due to the interaction of a relatively narrow magnetic mode (of the order of $\ell + 1$) with a broad electric mode (of the order of ℓ).

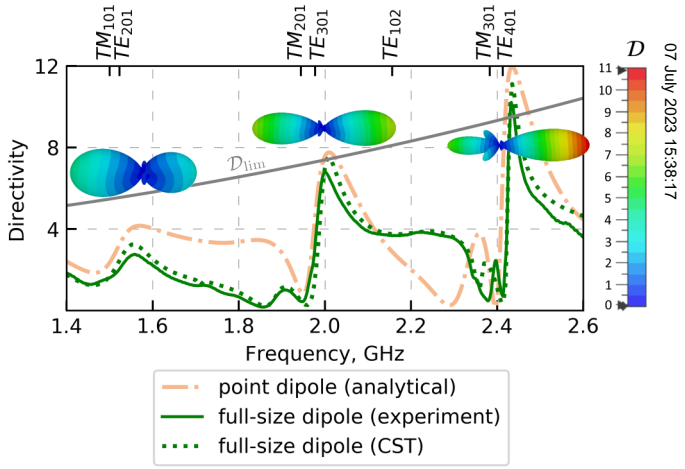

FIG. 3. Spectra of the directivity ($\mathcal{D}$) in the forward direction (along the z axis) in the range of 1.4–2.6 GHz for the cases of a full-size and point electric dipole oriented tangentially and located at a distance of $r_d = 40.5$ mm from the center of the spherical resonator with the radius of 40 mm. Antenna construction is described in Sec. III A. Calculations of the model with the point dipole were done with a proprietary code based on the theory developed in Ref. 14. The receiving horn antenna and the transmitting dipole antenna were located at a 3.4 m distance. Three-dimensional antenna patterns were obtained in the CST Studio Suite and correspond to the points of local maxima on the green dotted curve. The angular distribution of the directivity values corresponds to the color bar shown on the right. The ticks at the top of the graph correspond to the eigenmode frequencies of the spherical resonator used. The Kildal limit is shown with a solid gray line; the minimum radius of the sphere describing the antenna was assumed to be $R_{ant} = 50$ mm.

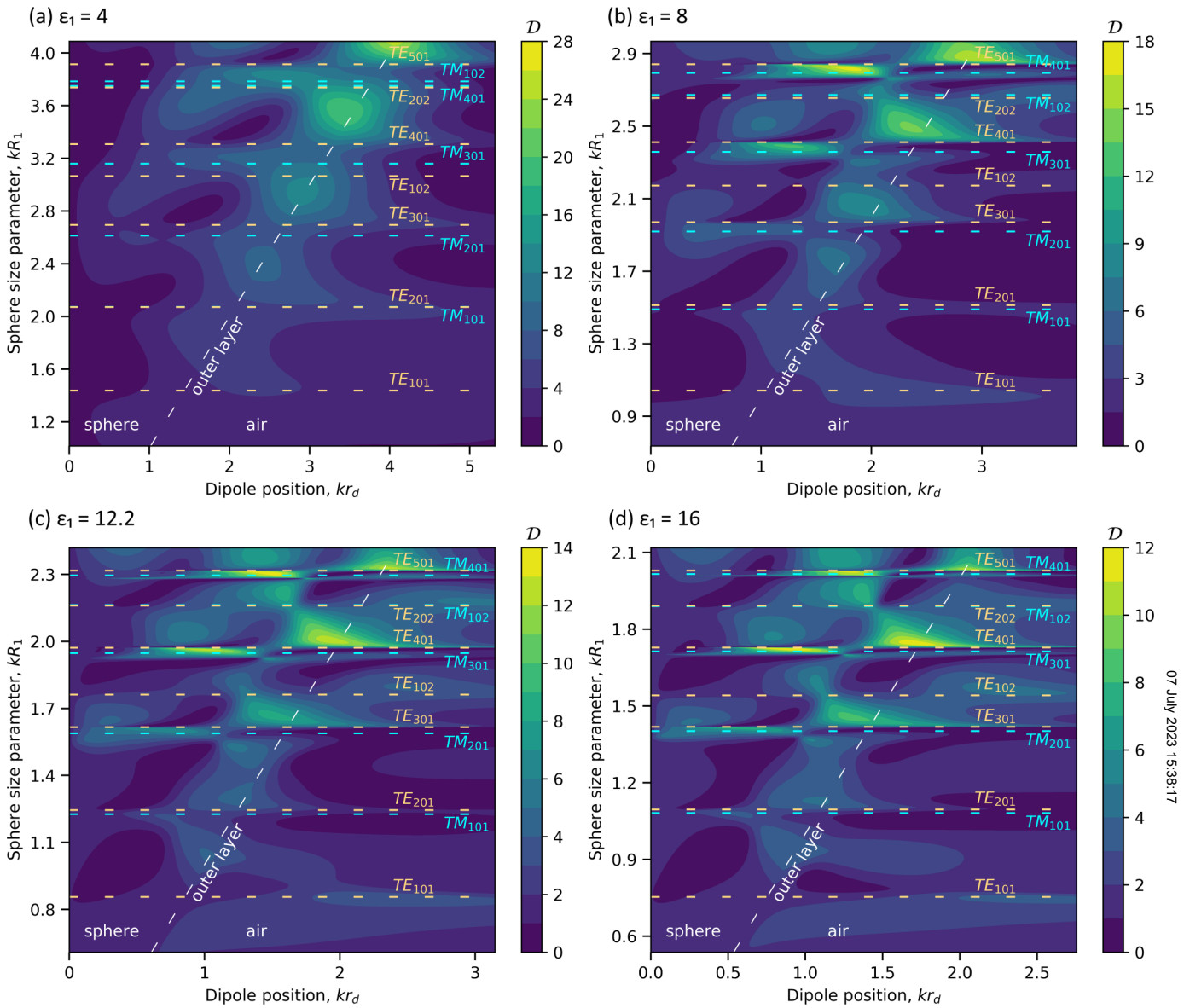

FIG. 4. Simulated dependence of the directivity in the forward direction (in a linear scale) of a spherical homogeneous dielectric resonator antenna on its dimensionless geometric size and the position of a tangentially oriented point dipole. Maps are presented for spheres with permittivity: (a) $\varepsilon_1 = 4$, (b) $\varepsilon_1 = 8$, (c) $\varepsilon_1 = 12.2$, and (d) $\varepsilon_1 = 16$. The position of the electric (TM) and magnetic (TE) eigenmodes of the spherical resonator is shown by dashed bright blue and peach horizontal lines, respectively. The dimensionless values of the sphere size parameter for the presented eigenmodes were obtained by solving Eq. (5).

Figure 2(c) shows numerical and experimental results for directivity, gain, and realized gain in a forward direction vs frequency. The data are given for the frequency range 2.3–2.6 GHz in the vicinity of the directivity resonance. The experimentally obtained directivity of the antenna reaches 10 at frequency 2.433 GHz. The half-power beamwidths (HPBWs) obtained numerically were equal to 47.3° and 34.1° for the $\phi = 0°$ and $\phi = 90°$ planes, respectively. In the experimental results, HPBWs were 48.6° and 35.5° for the indicated planes. There is a reasonable agreement between the experimental data calculated by formulas (2)–(4) and the simulation results obtained with the CST Studio Suite within the entire demonstrated frequency range. High total antenna efficiency is achieved at an antenna impedance close to 50Ω, resulting in minimal energy reflection back to the port and maximum radiation to the environment. The physics underlying the resonant directional behavior for the system under consideration is simultaneous excitation of the electric TM_{301} and magnetic TE_{401}

modes of the sphere by the electric dipole and constructive interference of the radiation in the forward direction. This is easy to check since for these two modes of the spherical resonator, the approximate relation $\zeta_{31} = \eta_1 k R_1 \simeq 6.988$ is satisfied [see Eq. (6)].

Figures 2(e) and 2(g) provide a comparison of the experimental and numerical radiation patterns in two planes ($\phi = 0°$ and $\phi = 90°$) for the resonant frequency of 2.433 GHz shown in Fig. 2(c). The difference between the experimentally measured and numerically calculated diagrams in Figs. 2(e) and 2(g) is associated with the effect of radiation from the coaxial cable feeding the antenna under test due to the currents arising on the cable surface: (i) for $\phi = 0°$ on the horizontal section of the cable and (ii) for $\phi = 90°$ on the vertical one. The radiation pattern outside the resonant frequency is affected also by sidelobes that arise uncontrollably due to the imperfection of the antenna.

B. Internal dipole

Although the use of a spherical resonator makes it possible to obtain the superdirectional radiation, the matched dipole located outside has a significant length and increases the overall size of the antenna (the circumscribing sphere). This makes it difficult to exceed Kildal's limit [Eq. (1)] while maintaining high total antenna efficiency. Therefore, we also considered the case of the electric dipole located inside a spherical dielectric resonator. The antenna with a dipole inside was made in the form of a plastic ball, similar to the antenna described above, but with an exciting electric dipole located inside, as shown in Fig. 2(b). The dipole was fixed in preperforated holes at three points of the plastic sheath: at the place where the cable crosses it and at the ends of the dipole arms. Then, the small gaps remaining in the holes were sealed with a hot glue, and after that, the powder was poured into the shell. Fabrication and measurement processes are presented in Sec. I of the supplementary material. The receiving horn antenna and the transmitting antenna were located at 2.7 m distance in this case.

The *internal* modes of a high-index dielectric spherical resonator are generally more efficiently excited from within its interior.[25] For an initial search of the optimal position of the dipole, a homogeneous spherical antenna excited by a tangentially oriented point dipole was considered. Figure 4 shows the directivity in the forward direction as a function of the dimensionless parameter of the antenna size and the dipole position for several values of permittivity. It is noticeable that with increasing the dielectric constant, the geometric size of the resonator decreases and the quality factor of the resonances increases. Figure 5 shows an enlarged fragment of Fig. 4(c) near the resonant condition of the TE_{401} mode. For the points with the maximum directivity, the dependence of the directivity on the angle θ in the planes $\phi = 0°$ and $\phi = 90°$ is plotted, and the corresponding multipole expansions are displayed. It turns out that the ratio of harmonic amplitudes is approximately the same for both the point dipole located inside and at the resonator boundary. By means of full-size optimization, the optimal position of the dipole is chosen on the z axis and shifted by 14.5 mm from the center of the sphere, which places the dipole arms near the zone with the highest directivity in Fig. 5 [marked point (a)]. The length of the dipole arms was 36 mm, and the gap between the centers of the cables was 4 mm. Such an experimental setup enables one to reduce the radius of the antenna circumscribing sphere down to 40 mm, i.e., to the size of the dielectric spherical resonator.

Figure 2(d) shows numerical and experimental results for directivity, gain, and realized gain as a function of frequency in the z-direction. The data are given for the frequency range of

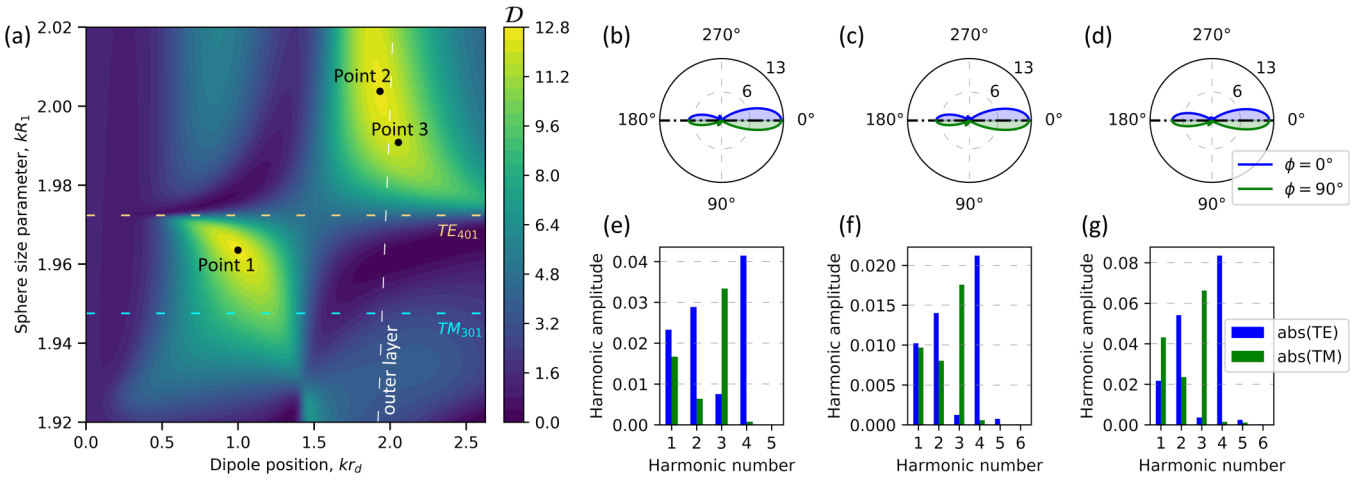

FIG. 5. (a) Simulated dependence of the directivity in the forward direction (in a linear scale) of a spherical homogeneous dielectric resonator antenna on its dimensionless geometric size and the position of a tangentially oriented point dipole for a fragment of Fig. 4(c) near the TE_{401} mode resonance. A map is presented for sphere with permittivity $\varepsilon_1 = 12.2$. The positions of the electric TM_{301} and magnetic TE_{401} eigenmodes of the spherical resonator are shown by dashed bright blue and peach horizontal lines, respectively. Polar plots (b)–(d) show the directivity vs polar angle θ for points 1, 2, and 3, respectively, marked on panel (a). The diagrams are axially symmetrical; therefore, two different planes are combined into one graph: the upper half shows the plane containing the dipole vector and the z axis ($\phi = 0°$), and the lower half describes the perpendicular plane ($\phi = 90°$). Below each polar plot, the corresponding multipole expansion is shown in (e)–(g).

2.2–2.5 GHz in the vicinity of the directivity resonance. The experimentally measured radiation patterns at the resonant frequency of 2.373 GHz in two planes are shown in Figs. 2(f) and 2(h). The directivity of the antenna reaches 9.1 in the direction $\theta = 0°$. The antenna exceeds the Kildal limit while maintaining high total antenna efficiency at the resonant frequency. The HPBWs that were numerically obtained are 45.9° and 44.5° for the $\phi = 0°$ and $\phi = 90°$ planes, respectively. In the experimental results, HPBWs are 47.5° and 40.1° for the indicated planes.

An increase in directivity can also be achieved for an external dipole by immersing the dipole under the outer surface of the resonator [point (b) in Fig. 5]. Using a small notch on the surface to place a dipole inside can also produce super-directional radiation, as has been numerically demonstrated in Ref. 32.

IV. DISCUSSION

Figure 6 shows a comparison of our results with the available experimental data (Fig. 3 of Ref. 45). Our results unambiguously demonstrate that it is possible to obtain both highly efficient and superdirective radiation simultaneously. Without taking into account the radiation efficiency, it is possible to arrive at even higher directivity values by about 15% for the same homogeneous sphere at a given resonance.

In view of potential applications, an assessment of antenna tolerances and possible sources of errors for both numerical and experimental data deserves particular attention. The analytical solution of an ideal point-like dipole problem of Ref. 14 can be reproduced with machine accuracy. For a more realistic description of the experimental setup, a three-dimensional electrodynamic problem was developed in the CST Studio Suite by means of the frequency domain solver.[62] Those simulations can also be tuned to yield numerically accurate solutions, though incremental changes

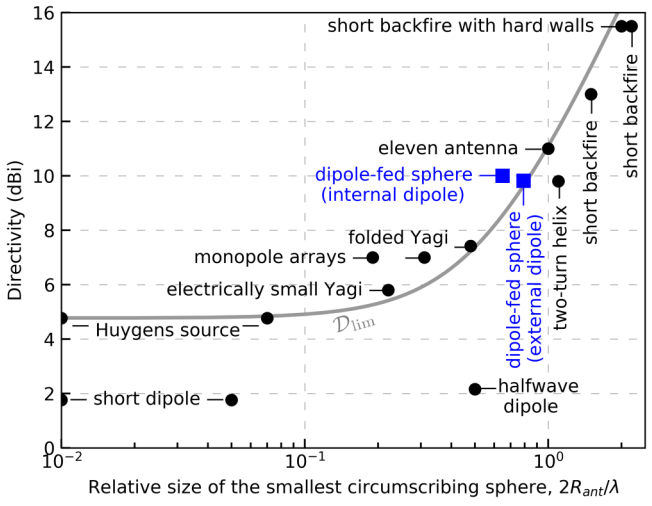

FIG. 6. Directivity of important antennas demonstrated in the literature (black circles)[45] and experimentally measured in this work (blue squares). The Kildal limit is shown with a solid gray line.

in some geometrical parameters, e.g., in a configuration of the feeding cables, were found to cause significant changes in the S-parameters in some spectral regions. Given that assessing these parameters experimentally is very difficult, there could be relatively large uncertainties related to their values even for relatively simple models as considered here.[57] Experimental data, including finite calibration tolerances (<1%), inaccuracies in the spatial orientation and position of the transmitting and receiving antennas (<1%), polarization loss (<0.2%), noise (<0.1%), parasitic reflections and radiation from equipment, not ideal parameters of the cables, dipole, and dielectric resonator, are the largest source of potential uncertainties and errors. Also, the directivity was evaluated with the S-parameters that were measured in only two planes ($\phi = 0°$ and $\phi = 90°$), which also bring an error related to the realistic pattern deviations when rotating around the z axis.

Surface irregularities and/or inhomogeneity of the sphere material lead to frequency splitting of excited modes with different magnetic number m, which leads to violation of the superdirectivity. Superdirective antennas have been in theory often considered with an infinite ground plane (see examples in Ref. 45), which is not taken into account when calculating the practical antenna size. However, in experimental realizations, this ground plane is comparable to the size of the antenna and can have a significant impact on the distribution of near fields.

Regarding practical realization of the directivity limit, a number of issues have to be taken into account. It is important to understand that the frequency bandwidth significantly decreases in the limit $\varepsilon_1 \to \infty$, which, together with the requirements on manufacturing quality, makes it impossible to use theoretically obtained resonances in practice. On the other hand, when $\varepsilon_1 \to 1$, it is as a rule impossible to excite well separated electric and magnetic modes of a spherical resonator at a given frequency. We believe that the value of $\varepsilon_1' = 12.2$ used in our experiment is a reasonable compromise for demonstrating the superdirectivity effect when operating at the required modes. At the same time, the value of $\varepsilon' = 12.2$ enables one to use silicon spheres when extending our results to telecommunication frequencies.

To design a super-directional antenna similar to the described one with the internal dipole, the following steps can be proposed. First, one should choose a sphere with a refractive index and size allowing for its TE_{401} eigenmode to be at a desired operating frequency [see Eqs. (5) and (6)]. Next, for the required kR, an approximate optimal dipole position is selected on the basis of point dipole approximation (see Fig. 4). Finally, a full-scale simulation and fine-tuning of the dipole parameters is carried out in order to minimize the return loss at the resonant frequency. The shape of the feed element can be further optimized to improve matching and reduce dependence on the position of the dipole inside the resonator.

Finally, it is important to mention the issue of the antenna bandwidth. This is an ambiguous parameter,[56] specifically for electrically small antennas. Typically, such antennas have low total radiation efficiency, whereas in our measurements, the radiation efficiency exceeded 80% within the 12 MHz frequency band, and the corresponding directivity reached the values of 8–10 for the case with an external dipole, and 6 – 9 for the case with an internal dipole.

V. CONCLUSION

The novelty of our work lies in that a spherical dielectric resonator can facilitate an antenna of a simple design having superdirectional radiation in a given direction. The use of high-index, low-loss ceramics allows one to significantly reduce the physical size of antennas, while maintaining high overall radiation efficiency and practical bandwidth. We have demonstrated both numerically and experimentally the possibility of superdirectional behavior for antennas smaller than the wavelength based on a spherical dielectric resonator with a dipole source. The antenna directivity is maintained at the frequencies of eigenmodes of the spherical resonator, provided that one appropriately adjusts the position of the dipole source. Our results can be extrapolated to a wide range of radio[65–69] and optical[34,70–73] frequencies with a suitable choice of high-index materials, while taking into account the cost, availability, and safety of the materials, as well as their compatibility with the desired manufacturing method. It should also be noted that reducing the size of the antenna leads to the main problem of all electrically small antennas, namely, the problem of impedance matching. Unfortunately, this problem is fundamental, and as the size decreases, the maximum achievable overall radiation efficiency of the antenna also decreases.[53,74,75] An ideal solution for this problem has not yet been obtained. Therefore, when the size of the antenna is greatly reduced relative to the wavelength, the maximum directivity can remain approximately the same, but the efficiency-dependent gain and the realized gain will decrease.

SUPPLEMENTARY MATERIAL

See the supplementary material for details related to the fabrication process of the antenna and more detailed data obtained during the measurements.

ACKNOWLEDGMENTS

The theoretical part of the work was supported by the Russian Science Foundation (Project No. 21-79-30038). The experimental part of the work was supported by the Priority 2030 Federal Academic Leadership Program.

AUTHOR DECLARATIONS

Conflict of Interest

The authors have no conflicts to disclose.

Author Contributions

Roman Gaponenko: Conceptualization (equal); Data curation (equal); Formal analysis (equal); Investigation (equal); Methodology (equal); Resources (equal); Software (equal); Validation (equal); Visualization (equal); Writing – original draft (equal); Writing – review & editing (equal). **Mikhail S. Sidorenko:** Investigation (equal); Resources (equal). **Dmitry Zhirihin:** Investigation (equal); Resources (equal); Writing – review & editing (supporting). **Ilia L. Rasskazov:** Conceptualization (equal); Writing – review & editing (equal). **Alexander Moroz:** Conceptualization (equal); Supervision (equal); Writing – review & editing (equal). **Konstantin Ladutenko:** Supervision (equal). **Pavel Belov:** Supervision (equal). **Alexey Scherbakov:** Conceptualization (equal); Formal analysis (equal); Software (equal); Writing - original draft (equal); Writing - review & editing (equal).

DATA AVAILABILITY

The data that support the findings of this study are available from the corresponding author upon reasonable request.

REFERENCES

[1]S. A. Long, M. W. McAllister, and L. C. Shen, IEEE Trans. Antennas Propag. **31**, 406 (1983).
[2]M. W. McAllister, S. A. Long, and G. L. Conway, Electron. Lett. **19**, 218 (1983).
[3]M. W. McAllister and S. A. Long, Electron. Lett. **20**, 657 (1984).
[4]P. Debye, Ann. Phys. **335**, 57 (1909).
[5]R. D. Richtmyer, J. Appl. Phys. **10**, 391 (1939).
[6]J. Stratton, *Electromagnetics Theory* (McGraw-Hill, 1941).
[7]M. Gastine, L. Courtois, and J. L. Dormann, IEEE Trans. Microw. Theory Tech. **15**, 694 (1967).
[8]M. Shafi, A. F. Molisch, P. J. Smith, T. Haustein, P. Zhu, P. De Silva, F. Tufvesson, A. Benjebbour, and G. Wunder, IEEE J. Sel. Areas Commun. **35**, 1201 (2017).
[9]Z. Zhang, Y. Xiao, Z. Ma, M. Xiao, Z. Ding, X. Lei, G. K. Karagiannidis, and P. Fan, IEEE Veh. Technol. Mag. **14**, 28 (2019).
[10]W. Lin, R. W. Ziolkowski, and J. Huang, IEEE Trans. Antennas Propag. **67**, 3670 (2019).
[11]H. Tataria, M. Shafi, A. F. Molisch, M. Dohler, H. Sjöland, and F. Tufvesson, Proc. IEEE **109**, 1166 (2021).
[12]J. Van Bladel, IEEE Trans. Microw. Theory Tech. **23**, 208 (1975).
[13]H. Chew, J. Chem. Phys. **87**, 1355 (1987).
[14]A. Moroz, Ann. Phys. **315**, 352 (2005).
[15]A. B. Evlyukhin, C. Reinhardt, A. Seidel, B. S. Luk'yanchuk, and B. N. Chichkov, Phys. Rev. B **82**, 045404 (2010).
[16]S. Arslanagic, M. Mostafavi, R. Malureanu, and R. W. Ziolkowski, in *Proceedings of the European Conference on Antennas and Propagation (EUCAP)* (IEEE, 2011), p. 2064.
[17]C. A. Balanis, *Advanced Engineering Electromagnetics*, 2nd ed. (John Wiley & Sons, Inc., 2012).
[18]A. E. Krasnok, C. R. Simovski, P. A. Belov, and Y. S. Kivshar, Nanoscale **6**, 7354 (2014).
[19]W. Liu, Opt. Express **23**, 14734 (2015).
[20]S. Arslanagić and R. W. Ziolkowski, IEEE Antennas Propag. Mag. **59**, 14 (2017).
[21]R. Li, X. Zhou, M. Panmai, J. Xiang, H. Liu, M. Ouyang, H. Fan, Q. Dai, and Z. Wei, Opt. Express **26**, 28891 (2018).
[22]I. L. Rasskazov, A. Moroz, and P. S. Carney, J. Opt. Soc. Am. A **36**, 1591 (2019).
[23]Z. Wang, B. Luk'yanchuk, L. Yue, B. Yan, J. Monks, R. Dhama, O. V. Minin, I. V. Minin, S. Huang, and A. A. Fedyanin, Sci. Rep. **9**, 20293 (2019).
[24]M. Majic and E. C. Le Ru, Appl. Opt. **59**, 1293 (2020).
[25]R. Gaponenko, A. Moroz, I. L. Rasskazov, K. Ladutenko, A. Shcherbakov, and P. Belov, Phys. Rev. B **104**, 195406 (2021).
[26]K. L. Wong, N. C. Chen, and H. T. Chen, IEEE Microw. Guided Wave Lett. **3**, 355 (1993).
[27]D. S. Filonov, A. E. Krasnok, A. P. Slobozhanyuk, P. V. Kapitanova, E. A. Nenasheva, Y. S. Kivshar, and P. A. Belov, Appl. Phys. Lett. **100**, 201113 (2012).
[28]A. B. Evlyukhin, S. M. Novikov, U. Zywietz, R. L. Eriksen, C. Reinhardt, S. I. Bozhevolnyi, and B. N. Chichkov, Nano Lett. **12**, 3749 (2012).
[29]A. I. Kuznetsov, A. E. Miroshnichenko, Y. H. Fu, J. Zhang, and B. Luk'yanchuk, Sci. Rep. **2**, 492 (2012).

[30]J. M. Geffrin, B. García-Cámara, R. Gómez-Medina, P. Albella, L. S. Froufe-Pérez, C. Eyraud, A. Litman, R. Vaillon, F. González, M. Nieto-Vesperinas, J. J. Sáenz, and F. Moreno, Nat. Commun. **3**, 1171 (2012).
[31]B. Rolly, J. M. Geffrin, R. Abdeddaim, B. Stout, and N. Bonod, Sci. Rep. **3**, 3063 (2013).
[32]A. E. Krasnok, D. S. Filonov, C. R. Simovski, Y. S. Kivshar, and P. A. Belov, Appl. Phys. Lett. **104**, 133502 (2014).
[33]A. E. Krasnok, E. A. Krasnok, D. S. Filonov, P. V. Kapitanova, and P. A. Belov, in *44th EuMC Rome, Italy* (IEEE Xplore, 2014), pp. 676–678.
[34]A. I. Kuznetsov, A. E. Miroshnichenko, M. L. Brongersma, Y. S. Kivshar, and B. Luk'yanchuk, Science **354**, aag2472 (2016).
[35]M. I. Tribelsky, J.-M. Geffrin, A. Litman, C. Eyraud, and F. Moreno, Sci. Rep. **5**, 12288 (2015).
[36]M. I. Tribelsky, J.-M. Geffrin, A. Litman, C. Eyraud, and F. Moreno, Phys. Rev. B **94**, 121110 (2016).
[37]Y. Tsuchimoto, T. Yano, T. Hayashi, and M. Hara, Opt. Express **24**, 14451 (2016).
[38]C. Forestiere, G. Miano, and G. Rubinacci, Phys. Rev. Res. **2**, 043176 (2020).
[39]I. Sinev, F. Komissarenko, I. Iorsh, D. Permyakov, A. Samusev, and A. Bogdanov, ACS Photonics **7**, 680 (2020).
[40]A. W. Powell, A. P. Hibbins, and J. R. Sambles, Appl. Phys. Lett. **118**, 251107 (2021).
[41]B. Rolly, B. Stout, and N. Bonod, Opt. Express **20**, 20376 (2012).
[42]R. W. Ziolkowski, Phys. Rev. X **7**, 031017 (2017).
[43]A. Monti, S. H. Raad, Z. Atlasbaf, and A. Toscano, Opt. Lett. **47**, 2386 (2022).
[44]P.-S. Kildal, in *Proceedings of the 2nd European Conference on Antennas and Propagation* [Institution of Engineering and Technology (IEEE), Edinburgh, UK, 2007], pp. 16–25.
[45]P.-S. Kildal, E. Martini, and S. Maci, IEEE Antennas Propag. Mag. **59**, 16 (2017).
[46]C. J. Bouwkamp and N. G. de Bruijn, Philips Res. Rep. **1**, 135 (1945).
[47]A. Uzkov, in *Comptes Rendus (Doklady) de l'Academie des Sciences de l'URSS* (USSR Academy of Science, Moscow, Russia, 1946), Vol. 53, pp. 35–38.
[48]E. Newman and M. Schrote, IEEE Trans. Antennas Propag. **30**, 1172 (1982).
[49]A. D. Yaghjian, T. H. O'Donnell, E. E. Altshuler, and S. R. Best, Radio Sci. **43**, RS3002 (2008).
[50]A. Haskou, A. Sharaiha, and S. Collardey, IEEE Antennas Wirel. Propag. Lett. **15**, 24 (2016).
[51]S. X. Ta, I. Park, and R. W. Ziolkowski, IEEE Access **5**, 14657 (2017).
[52]T. Shi, M.-C. Tang, R. Chai, and R. W. Ziolkowski, IEEE Trans. Antennas Propag. **70**, 5288 (2022).
[53]A. Karlsson, PIER **136**, 479 (2013).
[54]IEEE Std 145-2013 (Revision of IEEE Std 145-1993), 1 (IEEE, 2014).
[55]H. T. Friis, Proc. IRE **34**, 254 (1946).
[56]C. A. Balanis, *Antenna Theory: Analysis and Design*, 4th ed. (John Wiley & Sons, Inc., Hoboken, NJ, 2016).
[57]IEEE Std 149-2021 (Revision of IEEE Std 149-1977), 1 (IEEE, 2022).
[58]C. F. Bohren and D. R. Huffman, *Absorption and Scattering of Light by Small Particles* (John Wiley & Sons, 1998).
[59]P. C. Waterman, Phys. Rev. D **3**, 825 (1971).
[60]M. I. Mishchenko, *Electromagnetic Scattering by Particles and Particle Groups* (Cambridge University Press, 2014).
[61]*Handbook of Mathematical Functions with Formulas, Graphs, and Mathematical Tables*, edited by M. Abramowitz and I. A. Stegun (U.S. Department of Commerce, National Bureau of Standards, 1964).
[62]CST, Studio Suite® 2021; see https://www.3ds.com/products-services/simulia/products/cst-studio-suite/.
[63]W. Fan, A. Lu, L. L. Wai, and B. K. Lok, in *Proceedings of EPTC* (IEEE, 2003), pp. 533–537.
[64]Rohde & Schwarz, "Measuring balanced components with vector network analyzer ZVB" (2004), available at https://www.rohde-schwarz.com/us/applications/measuring-balanced-components-with-vector-network-analyzer-r-s-zvb-application-note_56280-15427.html.
[65]*Dielectric Resonator Antennas*, edited by K.-M. Luk and K.-W. Leung (SRP Ltd., Exeter, UK, 2003).
[66]S. B. Narang and S. Bahel, J. Ceram. Process. Res. **11**, 316 (2010).
[67]V. V. Parshin, E. A. Serov, E. E. Chigryai, B. M. Garin, R. N. Denisiuk, D. S. Kalyonov, M. Ding, L. Li, Y. Lu, Y. Yang, Y. Liang, J. Feng, and P. V. Ershova, J. Radio Electron. **2**, 1 (2018).
[68]*Dielectric Materials for Wireless Communication*, edited by M. T. Sebastian (Elsevier, 2008), Appendix II, pp. 541–652.
[69]H. Ohsato, J. Varghese, and H. Jantunen, in *Electromagnetic Materials and Devices*, edited by M.-G. Han (IntechOpen, Rijeka, 2018), Chap. 1.
[70]D. Smirnova and Y. S. Kivshar, Optica **3**, 1241 (2016).
[71]D. G. Baranov, D. A. Zuev, S. I. Lepeshov, O. V. Kotov, A. E. Krasnok, A. B. Evlyukhin, and B. N. Chichkov, Optica **4**, 814 (2017).
[72]D. Tzarouchis and A. Sihvola, Appl. Sci. **8**, 184 (2018).
[73]M. Odit, K. Koshelev, S. Gladyshev, K. Ladutenko, Y. Kivshar, and A. Bogdanov, Adv. Mater. **33**, 2003804 (2021).
[74]R. F. Harrington, J. Res. Natl. Bur. Stan. Sect. D Rad. Prop. **64D**, 1 (1960).
[75]R. C. Hansen, *Electrically Small, Superdirective, and Superconducting Antennas* (John Wiley & Sons, Inc., Hoboken, NJ, 2006).
[76]M. V. Rybin, P. V. Kapitanova, D. S. Filonov, A. P. Slobozhanyuk, P. A. Belov, Y. S. Kivshar, and M. F. Limonov, Phys. Rev. B **88**(20), 205106 (2013).